

SUPPLEMENTAL MATERIAL

Phase Control of Majorana Bound States in a Topological X Junction

Tong Zhou^{1,*}, Matthieu C. Dartiailh², William Mayer², Jong E.

Han¹, Alex Matos-Abiague³, Javad Shabani², and Igor Žutić^{1†}

¹*Department of Physics, University at Buffalo, State University of New York, Buffalo, New York 14260, USA*

²*Center for Quantum Phenomena, Department of Physics, New York University, New York 10003, USA*

³*Department of Physics and Astronomy, Wayne State University, Detroit, Michigan 48201, USA*

I. MAJORANA BOUND STATES IN A SINGLE PLANAR JOSEPHSON JUNCTION WITH ROTATED IN-PLANE MAGNETIC FIELD

Here we provide discussion about the results of the Majorana bound states (MBS) in a single planar Josephson junction (JJ) with rotated in-plane magnetic field, \mathbf{B} . Such a single JJ can be viewed as a special case of the X-shaped junction (XJ) when the two superconducting (S) regions are parallel, as shown in Fig. S1(a). Equivalently, this corresponds to the central angle $2\theta = 0$, defined between the two S regions in the Fig. 1 of the main text. Previous publications have reported that the topological superconductivity in planar JJs exists over a large parameter space when the magnetic field is along the S/normal region (N) interface [1–4]. Here we explore how the MBS evolve for in-plane B-field at a misalignment angle β with the S/N interface, introduced in Fig. S1(a). The corresponding Bogoliubov-de Gennes (BdG) Hamiltonian for the single JJ is the same as from the Eq. (1) in main text, but with the pairing potential, $\Delta(x)$, and chemical potential, $\mu(x)$, having one-dimensional dependences, written as

$$H = \left[\frac{\mathbf{p}^2}{2m^*} - \mu(x) + \frac{\alpha}{\hbar} (p_y \sigma_x - p_x \sigma_y) \right] \tau_z - \frac{g^* \mu_B}{2} \mathbf{B} \cdot \boldsymbol{\sigma} + \Delta(x) \tau_+ + \Delta^*(x) \tau_-, \quad (1)$$

where \mathbf{p} is the momentum, α is the Rashba spin-orbit coupling (SOC) strength, \mathbf{B} is the external magnetic field, μ_B is the Bohr magneton, while m^* and g^* are the electron effective mass and g -factor, respectively, taken a $m^* = 0.03m_0$,

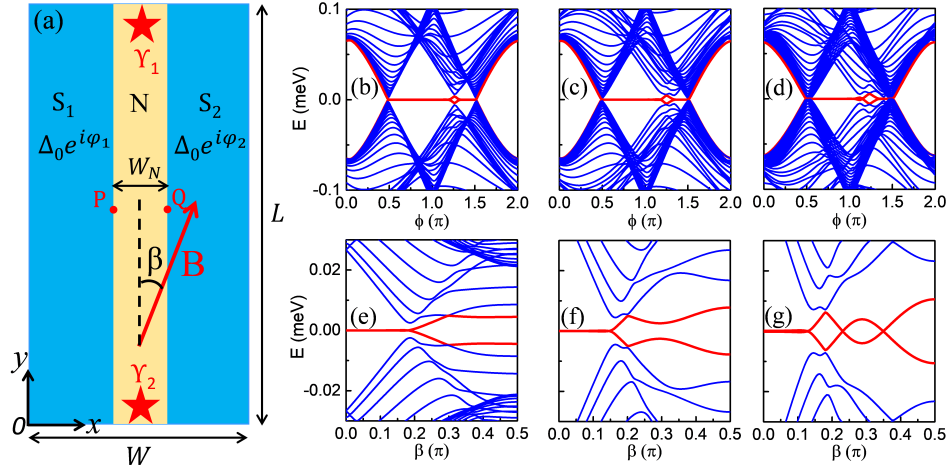


Fig. S 1. (a) Schematic of a planar Josephson junction with in-plane magnetic field, \mathbf{B} , at a misalignment angle β with the superconductor/normal region (S/N) interface. Two MBS, γ_1 and γ_2 , are denoted by stars at the opposite ends of the N region. P and Q denote the closest points at the edge of the opposite S regions, subsequently shown also in the X-shaped junctions. (b)-(d) Energy spectra with $B = 0.4$ T as a function of the superconducting phase difference, $\phi = \varphi_1 - \varphi_2$, for β of 0 , 0.1π , and 0.15π , respectively. (e)-(g) Energy spectra as a function of the angle β with the phase difference of $\phi = \pi$ for $B = 0.2$ T, 0.4 T, and 0.6 T, respectively. The red lines in the spectra indicate the evolution of finite-energy states into MBS inside the topological gap. The spectra were obtained for a junction with length $L = 3.2 \mu\text{m}$, width $W = 1.6 \mu\text{m}$ and $W_N = 100$ nm. The other parameters are the same as those in the Fig. 2. of the main text.

* tzhou8@buffalo.edu

† zigor@buffalo.edu

where m_0 is the electron mass, and $g^* = 10$ for InAs. We use τ_i (σ_i) as the Nambu (Pauli) matrices in particle-hole (spin) space and $\tau_{\pm} = (\tau_x \pm \tau_y)/2$. For the Zeeman term, we can write $\mathbf{B} \cdot \boldsymbol{\sigma} = \sigma_y B \cos \beta + \sigma_x B \sin \beta$ and the proximity-induced superconducting pairing potential for the 2DEG below the S leads,

$$\Delta(x) = \begin{cases} \Delta_0 \sqrt{1 - (B/B_c)^2} e^{i\varphi_1/2} & \text{for } 0 < x < (W - W_N)/2, \\ 0 & \text{for } (W - W_N)/2 \leq x \leq (W + W_N)/2, \\ \Delta_0 \sqrt{1 - (B/B_c)^2} e^{i\varphi_2/2} & \text{for } (W + W_N)/2 < x < W, \end{cases} \quad (2)$$

is expressed in terms of Δ_0 the superconducting gap, B_c the critical magnetic field, and the geometric parameters depicted in Fig. S1. For proximity-induced superconductivity in InAs we take $\Delta_0 = 0.23$ meV and $B_c = 1.6$ T for Al.

Solving the BdG Hamiltonian, we get the phase-difference biased energy spectra for different B-field orientation β , as shown in Fig. S1(b)-(d). As expected, the MBS emerge when $\beta = 0$ [Fig. S1(b)], in agreement with the previous work [1–4]. When β is increased, the phase-difference range supporting MBS becomes smaller [Figs. S1(c) and (d)]. However, even when β is up to 0.15π , there is still a large range of the phase difference (0.58π to 1.16π) supporting topological states [Fig. S1(d)]. To explore the range of β supporting MBS, we plot the β -dependent energy spectra of π -JJ in Fig. S1(e)-(g) for different values of magnetic field. As the misalignment angle increases, one can see the topological region is reduced and, eventually, fully suppressed, as observed experimentally [4]. However, the MBS would still survive for $B = 0.2$ T when the value of the misalignment angle is up to 0.2π , providing a useful guidance in designing XJs.

II. SUPERCONDUCTING AND NORMAL REGIONS IN X JUNCTIONS

By choosing the origin of the coordinate system at the lower-left corner, as shown in Fig. S2(a), for the proximity-induced superconductivity in a two-dimensional electron gas (2DEG), covered by an s -wave superconductor, we can describe four superconducting regions (S_1 , S_2 , S_3 , and S_4) and a normal region (N), uncovered by the superconductor, by the following relations,

$$S_1(x, y) = \begin{cases} y > \cot \theta (x - x_P) + y_P \\ y > -\cot \theta (x - x_Q) + y_Q \end{cases}, \quad S_2(x, y) = \begin{cases} y < \cot \theta (x - x_Q) + y_Q \\ y > -\cot \theta (x - x_Q) + y_Q \end{cases}, \quad (3)$$

$$S_3(x, y) = \begin{cases} y < -\cot \theta (x - x_P) + y_P \\ y < \cot \theta (x - x_Q) + y_Q \end{cases}, \quad S_4(x, y) = \begin{cases} y > \cot \theta (x - x_P) + y_P \\ y < -\cot \theta (x - x_P) + y_P \end{cases},$$

$$N(x, y) = \begin{cases} y \geq \cot \theta (x - x_Q) + y_Q \\ y \leq \cot \theta (x - x_P) + y_P \end{cases} \text{ or } \begin{cases} y \geq -\cot \theta (x - x_P) + y_P \\ y \leq -\cot \theta (x - x_Q) + y_Q \end{cases}, \quad (4)$$

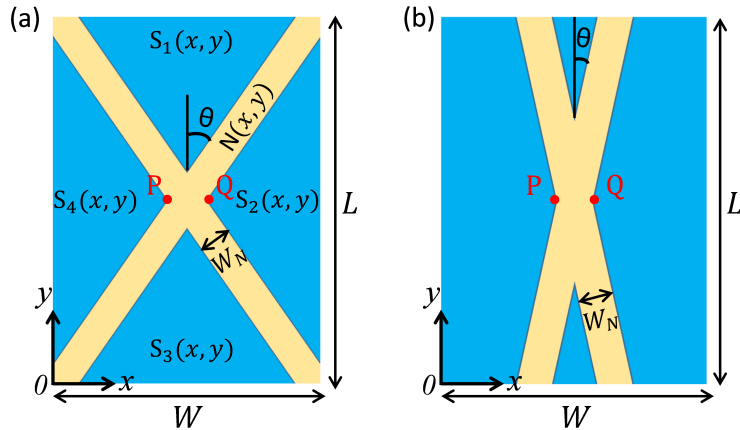


Fig. S 2. (a) Schematic of the XJ with position functions. P and Q points are the fixed crossing points. $S_1(x, y)$, $S_2(x, y)$, $S_3(x, y)$, $S_4(x, y)$, and $N(x, y)$ are the algebraic descriptions for S_1 , S_2 , S_3 , S_4 , and N regions, respectively. (b) Schematic of the XJ with the angle θ close to zero ($\tan \theta \ll W/L$).

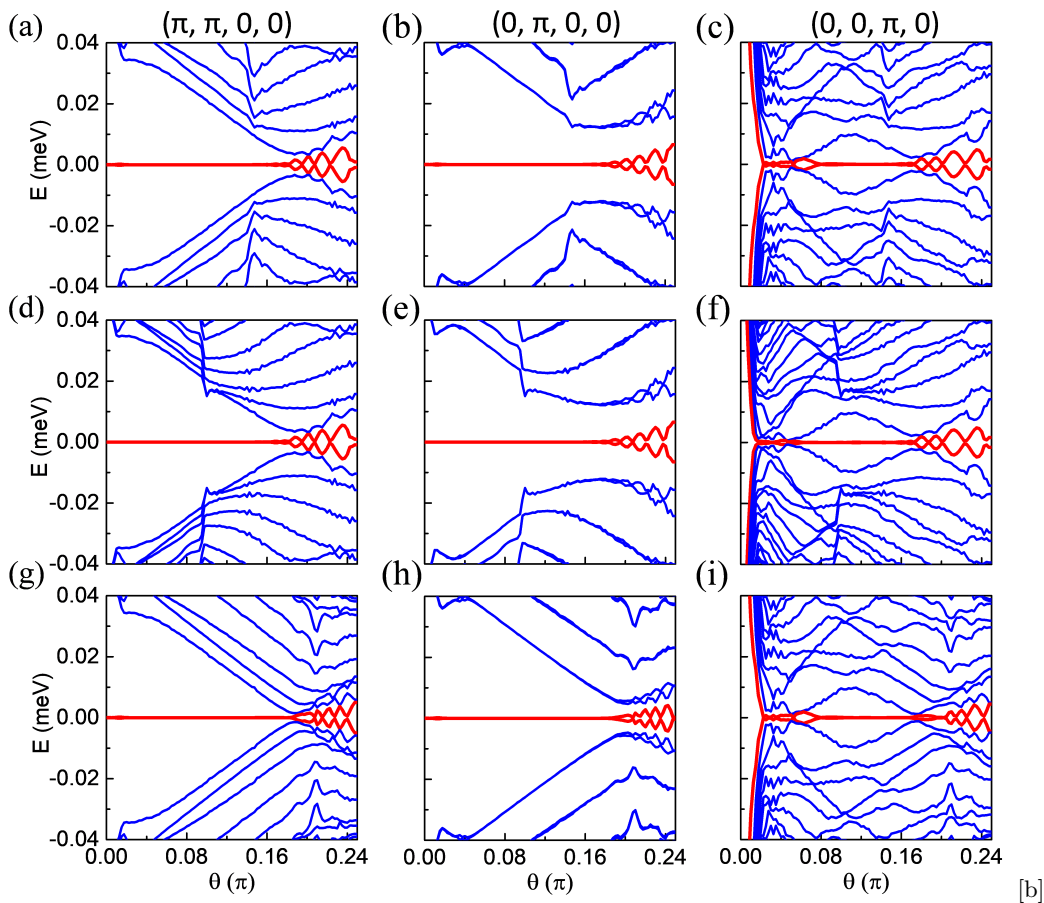


Fig. S 3. (a)-(c) Calculated energy spectra as a function of the central angle 2θ in XJs with $B = 0.4$ T for the diagonal $(\pi, \pi, 0, 0)$, long-edge $(0, \pi, 0, 0)$, and short-edge $(0, 0, \pi, 0)$ MBS types, respectively. The red lines indicate the evolution of the finite-energy states into MBS inside the topological gap. The geometric parameters are $L = 3.2 \mu\text{m}$, $W = 1.6 \mu\text{m}$, and $W_N/\cos\theta = 100$ nm. The other parameters, which are taken from Fig. 2 in main text. (d)-(f), are same as in panels (a)-(c), but with $L = 4.8 \mu\text{m}$. The parameters from panels (g)-(i) are the same as those in (a)-(c), but with $W = 2.4 \mu\text{m}$.

where (x_P, y_P) and (x_Q, y_Q) are the coordinates of the points P and Q , with $x_P = (W - W_N/\cos\theta)/2$, $x_Q = (W + W_N/\cos\theta)/2$, and $y_P = y_Q = L/2$. When θ is changed, the distance between the points P and Q points is fixed, but W_N varies, see Fig. S2(b). In the limiting case when θ is zero, the XJ becomes a single JJ, as shown in Fig. S1(a).

III. GEOMETRICAL EFFECTS IN X JUNCTIONS

In this Section we explore how the geometric parameters affect the MBS formation in XJs, especially as the central angle, 2θ , is changed. With the fixed system size, $L = 3.2 \mu\text{m}$, $W = 1.6 \mu\text{m}$, and $PQ = W_N/\cos\theta = 100$ nm, the distance between the crossing points, P and Q , we plot θ -dependent energy spectra in Fig. S3(a)-(c) for the diagonal, long-edge, and short-edge MBS types, respectively. When $\theta \sim 0$, the diagonal and long-edge configuration can be approximated by a single π -JJ where the MBS are stable for a large range of parameters [1–4]. Therefore MBS emerge in XJs as expected from the previously studied planar JJs, as shown in Figs. S3(a) and S3(b).

When θ is increased, the misalignment between the B-field along the y -direction and the S/N interface becomes larger. As a result of these less-favorable conditions, the MBS become fragile, which is consistent with the enhanced MBS oscillations. However, when θ is smaller than 0.18π , the MBS are stable for both configurations. Thus, the range of θ supporting diagonal and long-edge MBS are from 0 to 0.18π . For short-edge MBS, when $\theta \sim 0$, the areas of S_1 and S_3 are too small to support such MBS [see Fig. S2(b)]. As shown in Fig. S3(c), the MBS do not emerge until θ reaches 0.08π and become unstable when $\theta \approx 0.18\pi$. Thus, the range of θ supporting short-edge MBS is from 0.08π to 0.18π .

We also explore the influence of the system size of XJs. As shown in Fig. S3(d)-(i), increasing the XJ's length (L)

and width (W) does not give a clear change for all the three types of MBS (slightly suppress the oscillations of the zero-energy bands for short-edge MBS), indicating that the system size with $L \geq 3.2 \mu\text{m}$ and $W \geq 1.6 \mu\text{m}$ is already large enough to support MBS. With these results, we can identify that all the three MBS types can coexist in a robust form for θ from 0.08π to 0.18π with $L \geq 3.2 \mu\text{m}$ and $W \geq 1.6 \mu\text{m}$. Such a large parameter range gives a considerable flexibility for XJ fabrication. In fact the size of our fabricated XJ [see Fig. 1(b) in the main text] already fits well in this range of suitable geometric parameters, with $L = 4.0 \mu\text{m}$, $W = 2.0 \mu\text{m}$ and $\theta = 0.15\pi$.

IV. MBS EXCHANGE IN X JUNCTIONS

In this Section we provide complementary information about the MBS exchange by controlling the phase differences among the four S regions ($\varphi_1, \dots, \varphi_4$) with external fluxes Φ_1, Φ_2 , and Φ_3 , depicted in Fig. 1. In Figs. 3(f)-(j), we have shown the evolution of the calculated MBS probability densities from the diagonal [Fig. 3(a)] to a long-edge MBS [Fig. 3(b)] through continuously changing φ_1 from π to 0, but fixing $\varphi_2 = \pi$, $\varphi_3 = 0$, and $\varphi_4 = 0$ with external magnetic flux control. For this MBS evolution depicted in Fig. S4(a), we provide the corresponding low-energy spectra in Fig. S4(b). For any value of the continuously changing φ_1 , the MBS are protected by the topologically-nontrivial superconducting gap and remain stable during the whole switching time. As a result, the γ_2 can be adiabatically moved from the upper-left to the upper-right corner through the XJ center. We also provide an animation (see Diagonal2long.GIF) to show the whole process of the evolution of the MBS probability density for Fig. S4(a). Because of the XJ symmetry, the low-energy spectra of the evolution from long-edge MBS [Fig. 3(b)] to the other diagonal MBS [Fig. 3(c)] is same as that already shown in Fig. S4(b).

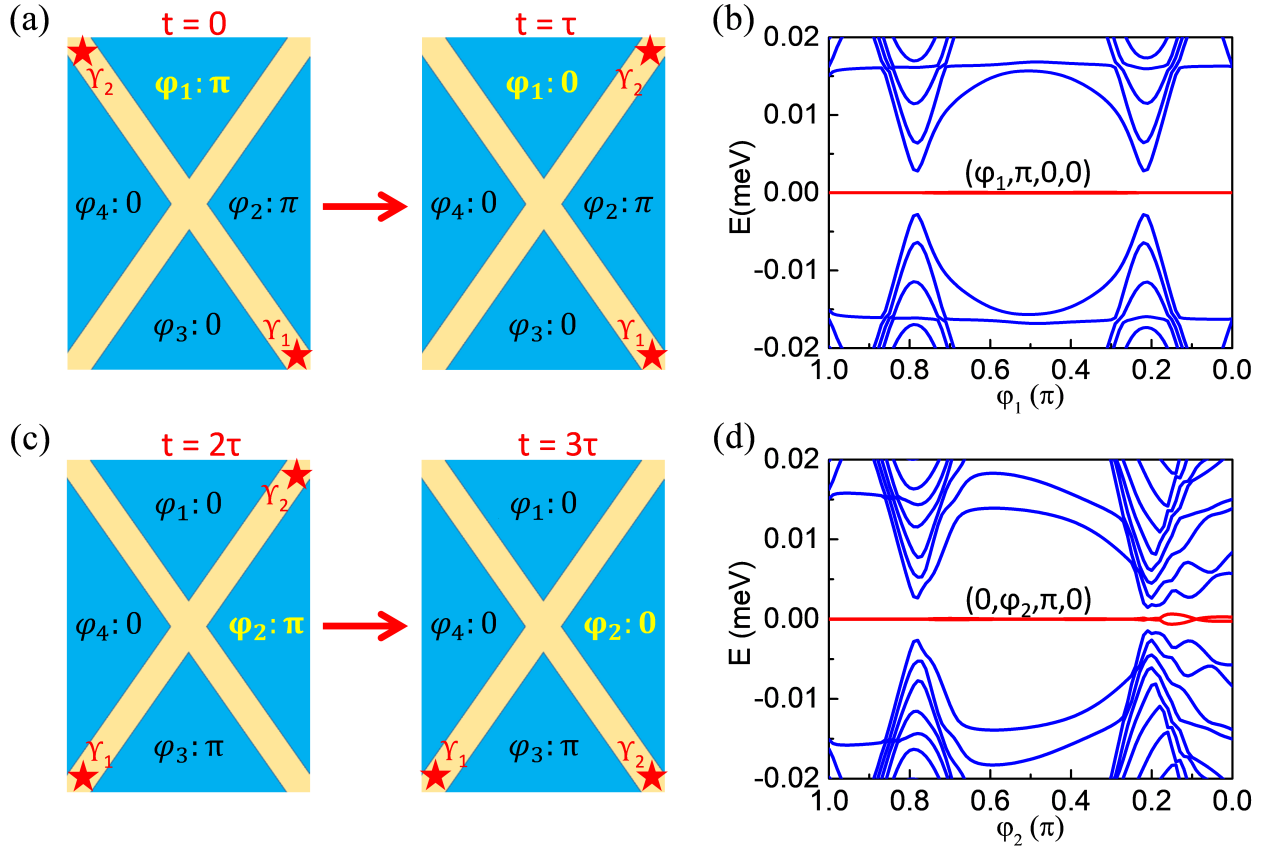


Fig. S 4. (a) Schematic of the evolution from the diagonal MBS [Fig. 3(a)] with $(\varphi_1, \varphi_2, \varphi_3, \varphi_4) = (\pi, \pi, 0, 0)$ to a long-edge MBS [Fig. 3(b)] with $(\varphi_1, \varphi_2, \varphi_3, \varphi_4) = (0, \pi, 0, 0)$. (b) The corresponding calculated spectra for (a) with continuously changing φ_1 from π to 0, but fixing $\varphi_2 = \pi$, $\varphi_3 = 0$, and $\varphi_4 = 0$. (c) Schematic of the evolution from the diagonal MBS [Fig. 3(c)] with $(\varphi_1, \varphi_2, \varphi_3, \varphi_4) = (0, \pi, \pi, 0)$ to a short-edge MBS [Fig. 3(d)] with $(\varphi_1, \varphi_2, \varphi_3, \varphi_4) = (0, 0, \pi, 0)$. (d) The corresponding calculated spectra for (c) with continuously changing φ_2 from π to 0, but fixing $\varphi_1 = 0$, $\varphi_3 = \pi$, and $\varphi_4 = 0$. The parameters are taken from Fig. 2.

We also provide a similar analysis for another step in the MBS exchange which is shown schematically in Fig. S4(c) as the evolution from the diagonal MBS [Fig. 3(c)] to a short-edge MBS [Fig. 3(d)] through continuously changing φ_2 from π to 0, but fixing $\varphi_1 = 0$, $\varphi_3 = \pi$, and $\varphi_4 = 0$. The corresponding evolution of the low-energy spectra is given in Fig. S4(d). Similar as in the previous step of the MBS exchange, for any value of the continuously changing φ_2 , the MBS are protected by the topologically-nontrivial superconducting gap and remain stable during the switching time. We provide the animation (see Diagonal2short.GIF) for the whole process of the evolution of the MBS probability density for Fig. S4(c). Invoking the XJ symmetry, the low-energy spectra of the evolution from Fig. 3(d) to Fig. 3(e) is same as shown Fig. S4(d), indicating that the short-edge MBS [Fig. 3(d)] can be adiabatically changed into the diagonal MBS [Fig. 3(e)]. These additional results and discussion corroborate that MBS in XJs can indeed be flexibly manipulated by the external flux control.

To realize the adiabatic evolution of the MBS exchange in Fig. 3, the switching time, τ , should be larger than the time τ_u , expected from the uncertainty relation, $\Delta E \tau_u \sim \hbar/2$, where ΔE is the energy gap between the ground state and first excited state. From our calculations in Fig. S4, the smallest ΔE is about $2 \mu\text{eV}$ during the whole process of MBS exchange, giving an estimated τ_u of approximately 0.17 ns. Thus, the switching time should exceed 0.17 ns to realize the adiabatic MBS evolution.

On the other hand, to avoid the quasiparticle poisoning, the switching time should be smaller than the quasiparticle poisoning time of the MBS, τ_p , in XJs. While, to the best of our knowledge, there are still no experimental measurements of τ_p in planar JJs, such τ_p is well explored in nanowire systems [5–7]. Specifically, $\tau_p \sim 1 \mu\text{s}$ is experimentally reported in Al/InAs system [5]. Considering that we analyze the same materials system, for the operation of XJs we also used $\tau_p \sim 1 \mu\text{s}$. Therefore, with $0.17 \text{ ns} < \tau < 1 \mu\text{s}$ we can apply the considered analysis to exchange the MBS in our XJ. Such condition on the relevant timescales can be readily achieved with external flux control, which eliminates the risk of excitation from the ground state and quasiparticle poisoning during the switching.

V. MBS FUSION IN X JUNCTIONS

In this Section, we show that XJs can be used to implement the fusion of MBS, which is an important step in demonstrating the non-Abelian character of MBS [8]. Figure S5(a) provides the flux protocol and the phase control for the fusion of the MBS. As shown schematically in Figs. S5(b)-(f), the diagonal MBS can be gradually moved and fused at the center of the XJ using the three external fluxes to change Φ_1 from 0 to $-0.25\Phi_0$ and then to change Φ_2 from $0.5\Phi_0$ to $0.25\Phi_0$ and Φ_3 from 0 to $0.25\Phi_0$, simultaneously, within the time 2τ , as shown in Fig. S5(a). Since we have shown in Fig. 4 of the main text that 4 MBS can be generated, a more complex fusion in XJ, for example, fusing (γ_1, γ_2) by changing φ_1 from π to 0 and fusing (γ_2, γ_3) by changing φ_2 from 0 to π can access different fusion channels, which could probe non-Abelian statistics [8].

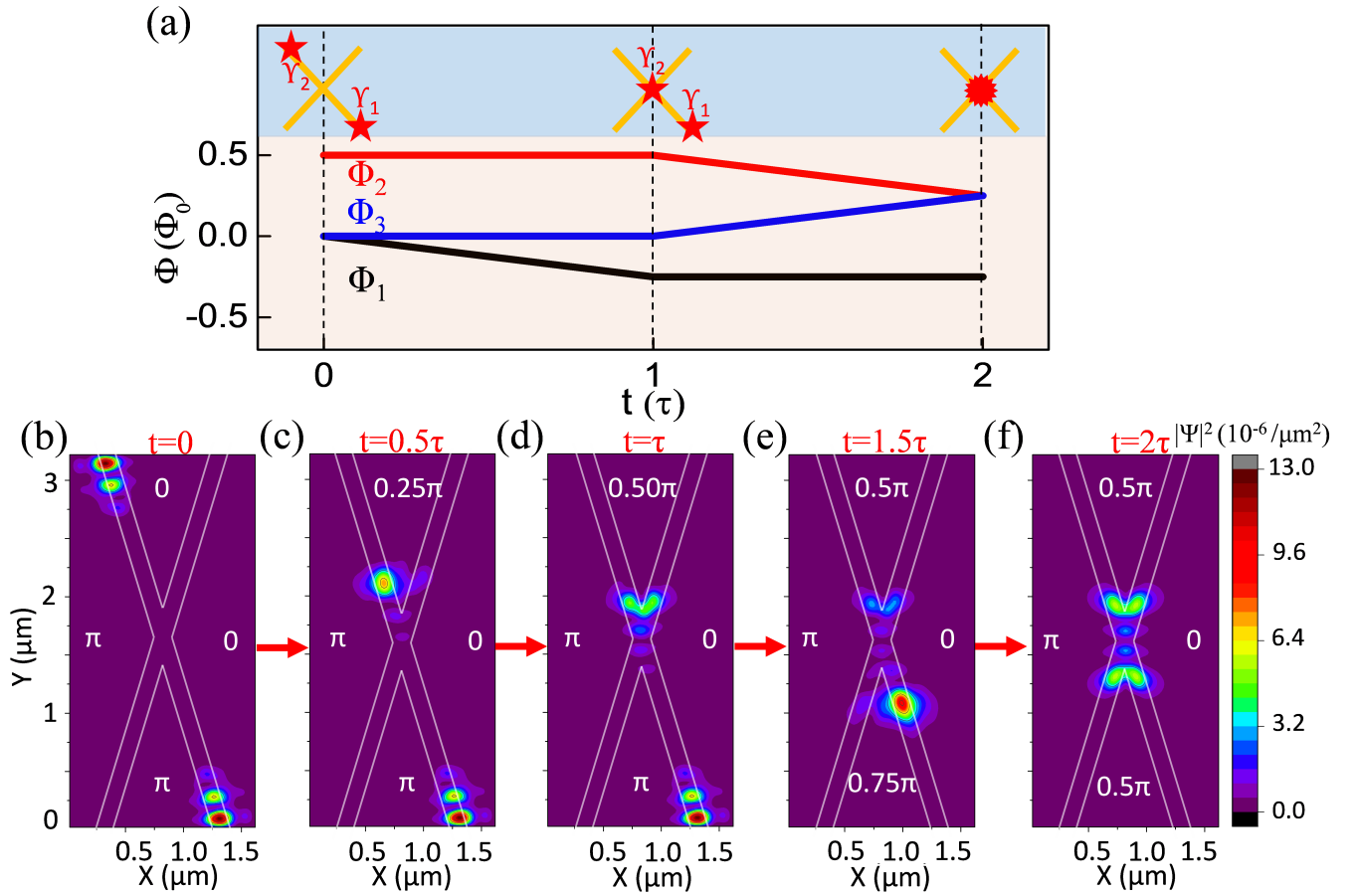


Fig. S 5. (a) Schematic of the flux protocol for the MBS fusion with external fluxes, τ is the switching time and Φ_0 is the magnetic flux quantum. (b) - (f) Calculated MBS probability densities for the MBS fusion. The parameters are taken from Fig. 3.

-
- [1] F. Pientka, A. Keselman, E. Berg, A. Yacoby, A. Stern, and B. I. Halperin, *Phys. Rev. X* **7**, 021032 (2017).
 - [2] H. Ren, F. Pientka, S. Hart, A. Pierce, M. Kosowsky, L. Lunczer, R. Schlereth, B. Scharf, E. M. Hankiewicz, L. W. Molenkamp, B. I. Halperin, and A. Yacoby, *Nature* **569**, 93 (2019).
 - [3] A. Fornieri, A. M. Whiticar, F. Setiawan., E. Portolés, A. C. C. Drachmann, A. Keselman, S. Gronin, C. Thomas, T. Wang, R. Kallaher, G. C. Gardner, E. Berg, M. J. Manfra, A. Stern, C. M. Marcus, and F. Nichele, *Nature* **569**, 89 (2019).
 - [4] W. Mayer, M. C. Dartiailh, J. Yuan, K. S. Wickramasinghe, A. Matos-Abiague, I. Žutić, and J. Shabani, arXiv:1906.01179 (2019).
 - [5] S. M. Albrecht, E. B. Hansen, A. P. Higginbotham, F. Kuemmeth, T. S. Jespersen, J. Nygård, P. Krogstrup, J. Danon, K. Flensberg, and C. M. Marcus, *Phys. Rev. Lett.* **118**, 137701 (2017).
 - [6] D. Rainis and D. Loss, *Phys. Rev. B* **85**, 174533 (2012).
 - [7] P. Aseev, J. Klinovaja, and D. Loss, *Phys. Rev. B* **98**, 155414 (2018).
 - [8] D. Aasen, M. Hell, R. V. Mishmash, A. Higginbotham, J. Danon, M. Leijnse, T. S. Jespersen, J. A. Folk, C. M. Marcus, K. Flensberg, and J. Alicea, *Phys. Rev. X* **6**, 031016 (2016).